

GALAXY CLUSTERS DISCOVERED WITH A SUNYAEV-ZEL'DOVICH EFFECT SURVEY

Z. STANISZEWSKI,^{1,2} P. A. R. ADE,³ K. A. AIRD,⁴ B. A. BENSON,⁵ L. E. BLEEM,^{6,7} J. E. CARLSTROM,^{6,7,8,9} C. L. CHANG,^{6,9} H.-M. CHO,⁵ T. M. CRAWFORD,^{6,8} A. T. CRITES,^{6,8} T. DE HAAN,¹⁰ M. A. DOBBS,¹⁰ N. W. HALVERSON,¹¹ G. P. HOLDER,¹⁰ W. L. HOLZAPFEL,⁵ J. D. HRUBES,⁴ M. JOY,¹² R. KEISLER,^{6,7} T. M. LANTING,¹⁰ A. T. LEE,^{5,13} E. M. LEITCH,^{6,8} A. LOEHR,¹⁴ M. LUEKER,⁵ J. J. MCMAHON,^{6,9} J. MEHL,⁵ S. S. MEYER,^{6,7,8,9} J. J. MOHR,¹⁵ T. E. MONTROY,^{1,2} C.-C. NGEOW,¹⁵ S. PADIN,^{6,8} T. PLAGGE,⁵ C. PRYKE,^{6,8,9} C. L. REICHARDT,⁵ J. E. RUHL,^{1,2} K. K. SCHAFFER,^{6,9} L. SHAW,¹⁰ E. SHIROKOFF,⁵ H. G. SPIELER,¹³ B. STALDER,¹⁴ A. A. STARK,¹⁴ K. VANDERLINDE,^{6,8,9} J. D. VIEIRA,^{6,7} O. ZAHN,¹⁶ AND A. ZENTENO¹⁵

Draft version September 1, 2022

ABSTRACT

The South Pole Telescope (SPT) is currently conducting a Sunyaev-Zel'dovich (SZ) effect survey over large areas of the southern sky, searching for massive galaxy clusters to high redshift. In this preliminary study, we focus on a 40 square-degree area targeted by the Blanco Cosmology Survey (BCS), which is centered roughly at right ascension $5^{\text{h}}30^{\text{m}}$, declination -53° (J2000). Over two seasons of observations, this entire region has been mapped by the SPT at 95 GHz, 150 GHz, and 225 GHz. We report the four most significant SPT detections of SZ clusters in this field, three of which were previously unknown and, therefore, represent the first galaxy clusters discovered with an SZ survey. The SZ clusters are detected as decrements with greater than 5σ significance in the high-sensitivity 150 GHz SPT map. The SZ spectrum of these sources is confirmed by detections of decrements at the corresponding locations in the 95 GHz SPT map and non-detections at those locations in the 225 GHz SPT map. Multiband optical images from the BCS survey demonstrate significant concentrations of similarly colored galaxies at the positions of the SZ detections. Photometric redshift estimates from the BCS data indicate that two of the clusters lie at moderate redshift ($z \sim 0.4$) and two at high redshift ($z \gtrsim 0.8$). One of the SZ detections was previously identified as a galaxy cluster using X-ray data from the ROSAT All-Sky Survey (RASS). Potential RASS counterparts (not previously identified as clusters) are also found for two of the new discoveries. These first four galaxy clusters are the most significant SZ detections from a subset of the ongoing SPT survey. As such, they serve as a demonstration that SZ surveys, and the SPT in particular, can be an effective means for finding galaxy clusters.

Subject headings: cosmology:cosmic microwave background – cosmology:observations – galaxies:clusters – Sunyaev-Zel'dovich Effect

Electronic address: tcrawfor@kicp.uchicago.edu

¹ Physics Department, Case Western Reserve University, Cleveland, OH 44106

² Center for Education and Research in Cosmology and Astrophysics, Case Western Reserve University, Cleveland, OH 44106

³ Department of Physics and Astronomy, Cardiff University, CF24 3YB, UK

⁴ University of Chicago, 5640 South Ellis Avenue, Chicago, IL 60637

⁵ Department of Physics, University of California, Berkeley, CA 94720

⁶ Kavli Institute for Cosmological Physics, University of Chicago, 5640 South Ellis Avenue, Chicago, IL 60637

⁷ Department of Physics, University of Chicago, 5640 South Ellis Avenue, Chicago, IL 60637

⁸ Department of Astronomy and Astrophysics, University of Chicago, 5640 South Ellis Avenue, Chicago, IL 60637

⁹ Enrico Fermi Institute, University of Chicago, 5640 South Ellis Avenue, Chicago, IL 60637

¹⁰ Department of Physics, McGill University, 3600 Rue University, Montreal, Quebec H3A 2T8, Canada

¹¹ Department of Astrophysical and Planetary Sciences and Department of Physics, University of Colorado, Boulder, CO 80309

¹² Department of Space Science, VP62, NASA Marshall Space Flight Center, Huntsville, AL 35812

¹³ Physics Division, Lawrence Berkeley National Laboratory, Berkeley, CA 94720

¹⁴ Harvard-Smithsonian Center for Astrophysics, 60 Garden Street, Cambridge, MA 02138

¹⁵ Department of Astronomy and Department of Physics, University of Illinois, 1002 West Green Street, Urbana, IL 61801

¹⁶ Berkeley Center for Cosmological Physics, Department of

1. INTRODUCTION

Galaxy clusters are the most massive collapsed objects in the universe, and measurements of their abundance and evolution can be used to place constraints on cosmological models. In particular, the abundance of clusters as a function of redshift depends on both the growth of structure and the volume of space. A catalog of clusters with masses and redshifts can be used to constrain the matter density, the density fluctuation amplitude, and the dark energy equation of state (Wang & Steinhardt 1998; Haiman et al. 2001; Holder et al. 2001; Molnar et al. 2004; Wang et al. 2004; Lima & Hu 2007).

For a galaxy cluster catalog to be useful for constraining cosmological models, the sample of clusters must be selected in a uniform and well understood manner (Melin et al. 2005). In addition, cluster parameters—mass, in particular—must be estimable from the observed quantities. Galaxy cluster catalogs selected via the Sunyaev-Zel'dovich effect are promising in both respects (Carlstrom et al. 2002; Majumdar & Mohr 2004; Melin et al. 2005).

The Sunyaev-Zel'dovich (SZ) effect is the inverse-

Physics, University of California, and Lawrence Berkeley National Labs, Berkeley, CA 94720

Compton scattering of Cosmic Microwave Background (CMB) photons by hot plasma bound to clusters of galaxies, which results in a distortion of the CMB blackbody spectrum (Sunyaev & Zeldovich 1970, 1972). The spectrum of the SZ effect has a null at ~ 217 GHz, where there is no net distortion and the intensity remains unchanged. At frequencies below ~ 217 GHz, the spectral distortion results in a decrement in the CMB intensity in the direction of the galaxy cluster.

As it is a distortion of the CMB spectrum, the surface brightness of the SZ effect does not depend on cluster distance. Observations of the SZ effect, therefore, permit the detection of clusters with a selection function that is nearly redshift-independent (Birkinshaw 1999; Carlstrom et al. 2002). The amplitude of the SZ spectral distortion is proportional to the integrated pressure along the line of sight through the cluster, and the relationship between integrated SZ flux and cluster mass is expected to have relatively low scatter (Motl et al. 2005; Nagai 2006; Shaw et al. 2007). Therefore, an SZ-flux-limited survey, combined with redshifts from optical observations, has the potential to be a nearly ideal data set for producing cosmological constraints.

Significant SZ detections of previously known clusters have been reported in many tens of X-ray and optically selected galaxy clusters with observations spanning from radio to submillimeter wavelengths (e.g., Jones et al. 2005; Bonamente et al. 2006; Benson et al. 2004; Halverson et al. 2008). However, despite the promise of SZ surveys for cosmology, there has been only one reported detection of the SZ effect in a field not already suspected to harbor a cluster. A deep survey of a relatively small field with the VLA at 8.4 GHz produced what appeared to be a significant flux decrement (Richards et al. 1997). However, subsequent BIMA observations at 30 GHz were found to be inconsistent with the interpretation of the VLA decrement as being due to the SZ effect (Holzapfel et al. 2000).

The South Pole Telescope (SPT) is the first instrument to demonstrate the requisite combination of resolution, mapping speed, and observing time to carry out a successful search for distant galaxy clusters through the SZ effect. The SPT is a 10-meter-diameter off-axis telescope optimized for observations of fine angular scale CMB anisotropy (Ruhl et al. 2004; Padin et al. 2008; Carlstrom et al. 2008). The SPT receiver is equipped with a 960-element array of superconducting transition edge sensor (TES) bolometers, read out by frequency-domain-multiplexed superconducting quantum interference device (SQUID) amplifiers. This array is made up of six sub-arrays, each of which can be configured to observe in one of the 95, 150, or 225 GHz atmospheric windows. The SPT has begun an extensive survey of the high-galactic-latitude sky visible from the South Pole. This paper presents the four most significant detections of SZ clusters in a preliminary analysis of a ~ 40 square-degree subset of the SPT survey area.

Descriptions of the SPT observations, data reduction, and cluster-searching algorithms are found in Section 2. The cluster candidates are presented in Section 3, including a discussion of possible X-ray counterparts in Section 3.1 and optical followup observations in Section 3.2. Finally, we summarize the main results of this work in Section 4.

2. OBSERVATIONS AND DATA REDUCTION

The results presented in this work are based on observations of a single field, using data collected over two seasons. In the combined data set, the field is fully covered in our three frequency bands. Details of the observations are given in Section 2.1. For each of the few hundred individual observations,¹⁷ initial data cuts are performed, various timestream processing steps are applied, and a single map is made using the data from all selected detectors in a given observing band. The maps from each individual observation are combined to produce a single map of the observed region in each band. Details of the data reduction up to the final maps are given in Section 2.2. Finally, the most sensitive single-frequency map is searched for SZ cluster candidates using a matched-filter technique, the details of which are given in Sections 2.3 and 2.4.

2.1. Observations

The observations included in this analysis were performed during the 2007 and 2008 SPT observing seasons, using a different focal plane configuration each season. Both the 2007 and 2008 focal planes included detectors sensitive to radiation within bands centered at approximately 95 GHz, 150 GHz, and 225 GHz. Details of the telescope design and performance, focal-plane configuration, and observing strategy for these two seasons are described in Carlstrom et al. (2008). During the 2007 Austral Winter, the SPT began a survey of a ~ 40 square-degree field that was also targeted by the Blanco Cosmology Survey¹⁸ (BCS) project. This field is centered roughly at right ascension (R.A.) $5^{\text{h}}30^{\text{m}}$, declination (decl.) -53° (J2000) and is hereafter referred to as the BCS5h30 field. The observations of the BCS5h30 field with the 2007 SPT focal plane that are included in this paper took place between July 27 and September 19, 2007, for a total of 280 hours of observing time. From this period, we use only the 95 GHz data taken with detectors that passed a set of performance cuts, yielding a median of 129 well-performing detectors per observation.

Between February 29 and June 5, 2008, a ~ 90 square-degree field including the BCS5h30 field was observed with the 2008 SPT focal plane. For this paper, we include 607 hours of observing time on the ~ 90 square-degree field with a median of 322 good 150 GHz detectors and 170 good 225 GHz detectors. We report results only for the subset of this larger field that overlaps the BCS5h30 field.

The observations reported here were performed using constant-elevation scans across the field. In this scan strategy, the entire telescope is swept at constant angular velocity in azimuth from one edge of the field to the other, and then back. After each such pair of scans across the field, the telescope executes a step in elevation before performing the next pair. A scanning speed of 0.84 degrees of azimuth per second was chosen for the 2007 observations presented here. The 2008 observations employed two different scan speeds, 0.44 and 0.48 degrees of azimuth per second. The size of the elevation step

¹⁷ In this work, we refer to an observation as a single-pass map of the entire field.

¹⁸ <http://cosmology.uiuc.edu/BCS/>

between pairs of scans was 0.07 degrees for the 2007 observations and 0.125 degrees for the 2008 observations. A map of the entire field is made using this strategy, and we refer to such a single-pass map as a single observation. One observation takes up to two hours. The short time period for a single observation allows for a conservative schedule of interleaved calibrations and facilitates data selection and reduction. Each individual observation produces a fully sampled map of the field, but not fully sampled by each individual detector. A series of different starting elevations are used for successive observations to provide even, fully sampled, coverage of the field over several days.

Between individual observations of the field, we perform a series of short calibration measurements described in more detail in Carlstrom et al. (2008). These include measurements of a chopped thermal source, ~ 2 degree elevation nods, and scans across the galactic HII regions RCW38 and MAT5a. This series of regular calibration measurements allows us to identify detectors with good performance, assess relative detector gains, monitor atmospheric opacity and beam parameters, and constrain pointing variations.

2.2. Data Reduction

For this initial cluster-finding analysis, a preliminary data reduction pipeline was developed that provides maps of the BCS5h30 field that are well understood, but not yet optimized. Details of the data processing as presented below are subject to improvement for future analysis.

2.2.1. Data selection and notch filtering

The first step in the data reduction process is to identify the data that will be included in each single-observation map. For every observation, a set of well-performing detectors is identified, primarily by assessing each detector’s response to the chopped thermal source, its response to atmospheric emission during the ~ 2 degree elevation nods, and its noise in the frequency band appropriate for cluster signals. Performance is also assessed based on the shape of the individual detector’s noise power spectrum. If the power spectrum has too many lines or other deviations from the expected functional form, that detector is omitted from that observation’s analysis. The median number of detectors stated in Section 2.1 is obtained after the application of these criteria.

In addition to cutting all data from individual detectors with anomalous noise power spectra, a small amount of bandwidth is cut from all detectors in certain observations. The 2008 receiver exhibits sensitivity to the pulse-tube cooler, resulting in occasional lines in the detector noise power spectra at frequencies corresponding to the pulse-tube frequency (approximately 1.6 Hz) and its harmonics. In every observation, all detectors’ noise power spectra are combined in quadrature, and a search is performed for features in the resulting spectrum at every harmonic of the pulse-tube frequency. If a high-significance feature is found at any harmonic, a notch filter around that harmonic is applied to every detector’s timestream. The width of the notch is determined by the fit, with a maximum of 0.007 Hz full-width. The maxi-

um amount of bandwidth that could be cut with this filter is 0.4%, but the actual amount is far smaller.

The data are eventually parsed into individual azimuth scans and are further selected for inclusion in the analysis on a scan-by-scan basis. Only the constant-azimuthal-velocity portion of each scan is eligible for inclusion; data taken while the telescope is accelerating are omitted. Scans during which there were data acquisition problems or abnormally large pointing errors—roughly 5% of total scans—are flagged for omission. For each detector, data from an individual scan are flagged if the detector or its associated readout channel exhibits high noise, if the demodulated detector output comes close to the limits of the analog-to-digital converter, if the readout SQUID associated with the detector exhibits an anomalously large DC offset, or if the detector demonstrates any cosmic ray-like events in its time-ordered data. Typically about 5% of all otherwise well-performing bolometers are flagged within a given scan for one of these reasons. Data that remain unflagged after all of these cuts have been applied are processed and included in the maps.

Finally, individual observations are assessed for quality before inclusion in the final coadded maps. Observations are excluded if the thermal conditions of the receiver were not sufficiently stable, if the number of well-performing detectors was anomalously low, or if the observation was not fully completed. Individual observation maps are also excluded from the final maps if the RMS in the single-observation map exceeds an empirically determined threshold. Of the complete observations of the BCS5h30 field, approximately 77% (270/350) of the 2007 observations and 83% (314/377) of the 2008 observations are included in the final maps.

2.2.2. Relative and absolute calibration

The relative gains of the detectors, and their gain variations over time, are estimated using measurements of their response to a chopped thermal source taken before every observation. This relative calibration is used to “flat-field” the array before estimation of any common-mode timestream signal and before mapmaking. For the relative calibration step before mapmaking, we apply corrections to account for variations in illumination of the thermal source across the focal plane. These are measured by calculating the ratio of each detector’s response to the thermal source to its response to the galactic HII region RCW38, averaged over many measurements.

We convert the RCW38-corrected relative calibration into an absolute calibration by comparing our measurements of RCW38 with published flux measurements in our observing bands. For 150 and 225 GHz, we compare to the RCW38 flux reported by ACBAR (Runyan et al. 2003), which was recently linked to the WMAP5 calibration at 150 GHz (Reichardt et al. 2008). In order to use the ACBAR calibration, we smooth the SPT map of RCW38 to match the ACBAR resolution. We then compare the flux within the inner 8 arcminutes of the SPT map with the ACBAR-determined flux. For the 95 GHz calibration, we use the flux reported by BOOMERANG (Coble et al. 2003). In this case, we smooth the SPT RCW38 map to match the BOOMERANG resolution and then compare the flux within two times the Gaussian width (σ) of the BOOMERANG beam.

This calibration method does not correct for temporal

variations in atmospheric opacity between SPT measurements of RCW38. This results in a slightly sub-optimal weighting of detectors during map-making, but does not bias the absolute calibration. The added absolute calibration uncertainty from ignoring atmospheric opacity corrections is small relative to our overall calibration uncertainty. For each of our bands over both seasons, the RMS variation in the brightness of RCW38 is measured to be $< 5\%$, even without correcting for differences in atmospheric opacity or changes in the relative response of the bolometers.

We estimate the calibration uncertainty of the 95, 150, and 225 GHz bands to be 13%, 8%, and 16%, respectively. At these levels of uncertainty, the RCW38-based calibration is consistent with other cross-checks of our calibration, including initial CMB power spectrum estimates and observations of Neptune.

2.2.3. Timestream processing

In addition to the notch filtering described in Section 2.2.1, the timestream processing of detector data consists of deconvolution of the detector response function, low-pass filtering, and projecting out long-timescale drifts due to atmosphere and readout $1/f$ noise.

Detector-response deconvolution and low-pass filtering are done in a single step. The detector temporal-response functions are measured periodically by sweeping the chop frequency of the thermal calibration source and measuring the amplitude and phase of each detector's response. These temporal-response functions are fit well by a single-pole low-pass filter, and the time constants do not vary significantly from observation to observation. Across the focal plane, the time constants ranged from 5-10 ms in 2007 and from 10-20 ms in 2008. The cutoff for the applied low-pass filter is set at 40 Hz for the 2007 data and 25 Hz for the 2008 data, such that in conjunction with a digital filter already applied by the data acquisition computer, they filter approximately the same spatial scales ($\lesssim 0.5$ arcminutes), given the different scan speeds for each season. This combination acts as an anti-aliasing filter for our eventual resampling of the data onto 0.25-arcminute map pixels but does not suppress power on scales of the SPT beams.

For every scan, each detector's timestream is then fit simultaneously to a number of slowly varying template functions, and the best fit to each template is subtracted from that detector's timestream. This time-domain filter reduces the effect of low-frequency noise in the detector timestreams due to readout noise or to atmospheric fluctuations. For this analysis, we use a combination of Legendre polynomials and an array common mode as the templates. The highest order of Legendre polynomial used is 19 for the 2008 data and 11 for the 2007 data, resulting in a characteristic filter scale of roughly one half degree for both seasons.

The common-mode template is constructed from the mean across all the well-performing detectors in the array at a given observing frequency, using a nominal relative calibration. Removing this common mode should eliminate the majority of the atmospheric fluctuation power in the detector timestreams, because this atmospheric signal is highly correlated between detectors. The common-mode subtraction acts as a spatial high-pass filter with a characteristic scale that roughly corresponds to the one

degree angular size of the array.

In order to avoid contamination of the best-fit common mode and polynomial by bright point sources, sources were detected in a preliminary set of maps, and the locations of those sources were masked in the common mode and polynomial subtraction algorithm. A total of 92 sources were masked in this analysis, 35 of which lie in the ~ 40 square-degree BCS5h30 field. A mask radius of 5 arcminutes was used for the 5 brightest sources (including the 3 brightest in the BCS5h30 field), and a mask radius of 2 arcminutes was used for the rest.

2.2.4. Mapmaking and pointing corrections

For every observation, a map is made for each observing frequency using the processed data for all detectors in that band. Pointing information (R.A. and decl.) is calculated for each detector using focal-plane offsets measured in observations of the galactic HII regions, and boresight pointing calculated using data from the telescope pointing readout system, with a set of corrections described below. Pointing coordinates are converted to pixel number using a Sanson-Flamsteed projection (Calabretta & Greisen 2002) with 0.25-arcminute pixels, and all measurements of a given pixel's brightness are averaged using inverse-variance weighting based on the RMS of each detector's processed and relative-gain-scaled time-ordered data.

Small corrections must be applied to the pointing information in the timestream to ensure that pointing errors are suitably small compared to the size of the SPT beams. The largest pointing errors of the SPT are attributed to thermal gradients across the telescope support structure. These pointing errors are corrected from 20 arcseconds RMS to better than 8 arcseconds RMS by using an offline model which incorporates information from thermal and linear displacement sensors on the telescope structure and observations of HII regions. The astrometry of the pointing model is tied to the PMN and SUMSS catalogs (Wright et al. 1994; Mauch et al. 2003) and is accurate to 10 arcseconds in the final maps. The beams in the final maps are well approximated by 2D elliptical Gaussians with average full widths at half maximum (FWHM) of 1.5, 1.2, and 1.1 arcminutes for 95, 150, and 225 GHz. As the beams include the effects of pointing variations and the timestream filtering, they are larger than expected from the diffraction of the central 8-meter diameter region of primary mirror illuminated by the SPT-SZ optics (see Padin et al. 2008).

2.3. Identifying Galaxy Cluster Candidates

In this initial analysis, we identify the highest-significance clusters using only the 150 GHz map, which has the highest sensitivity. The maps at the other two frequencies are used to provide a cross check of the cluster detections. The cluster thermal SZ signal should nearly vanish in the 225 GHz map, while the 95 GHz map can be used to confirm the detected clusters. We enhance the signal to noise in the SPT maps for sources with morphologies similar to that expected for SZ galaxy clusters through the application of matched spatial filters (Haehnelt & Tegmark 1996; Herranz et al. 2002a,b; Melin et al. 2006). The matched filter, which we apply in the Fourier domain, combines knowledge of the source template with a noise estimate to optimize the signal-to-noise

of the source in the filtered map:

$$\psi = \frac{S^T N^{-1}}{\sqrt{S^T N^{-1} S}} \quad (1)$$

where ψ is the matched filter, N is the noise covariance matrix (including non-SZ foregrounds) and S is the assumed source template.

2.3.1. Source Templates

The optimal choice for the source template is unclear for SZ clusters, so we explore three basic profiles, all motivated by some guess at the underlying 3-dimensional pressure profile of clusters: a modified version of the NFW (Navarro et al. 1996, 1997) model as suggested in Nagai et al. (2007), numerically integrated along the line of sight to produce a model for the SZ surface brightness; a Gaussian profile; and a β -model with β between 2/3 and 4/3, which can be analytically integrated to yield the SZ surface brightness. The three models proved almost indistinguishable in terms of detecting the highly significant clusters presented in this work. The results in Section 3 are based on a spherical β -model with $\beta = 1$. The SZ surface brightness profile using a β -model is given by

$$\Delta T_{SZ}(\theta) = \Delta T_0 (1 + \theta^2 / \theta_{\text{core}}^2)^{(1-3\beta)/2}, \quad (2)$$

where θ is the angular distance from the line of sight through the center of the cluster, θ_{core} is the (angular) core radius, and ΔT_0 is the peak signal. We choose to fix β and vary θ_{core} , as these two parameters are highly degenerate in the fit, given the current depth and resolution of our observations. The model is truncated at $10 \times \theta_{\text{core}}$. We have explored the dependence on the scale size, parametrized as θ_{core} in the range from 0.25' to 3.5' in 0.25' steps, and generated a matched filter of each case.

The timestream filtering described in Section 2.2.3 affects the expected shape of the cluster signal in our maps. To account for this effect, we convolve the source templates with a spatial filter intended to represent the map-domain version of our timestream filtering before including the source templates in the matched filter for cluster detection. The spatial filter used in this work is simply a high-pass in the R.A. direction, with a cutoff on roughly half-degree scales. Simulations of the timestream filtering have shown this to be an accurate representation of the effect of our timestream polynomial removal. We do not attempt to include the effects of our common-mode subtraction, which predominantly affects modes that will be heavily de-weighted in the matched filter by the inclusion of the primary CMB as a noise term.

2.3.2. Noise and Foreground Estimates

In addition to the SZ signal from massive clusters, SPT maps contain primary CMB, instrument and atmospheric noise, point sources, and an unresolved SZ background. For cluster detection, all of these are noise sources. The covariance matrix used to create the optimal matched filter can be expressed as the sum, $N = N_{\text{CMB}} + N_{\text{noise}} + N_{\text{PS}} + N_{\text{SZ}}$, of these components. The point-source covariance only includes the unresolved source background; point sources bright enough to be detected in our maps are treated separately as discussed below.

The signal covariance of the primary CMB and undetected point sources is estimated analytically from the best-fit WMAP5 CMB power spectrum (Nolta et al. 2008) and the Borys et al. (2003) model for dusty point sources. We assume that the contribution of faint radio sources to the background source covariance is negligible. We assume a spectral index of 2.7 to extend the dusty source counts to 150 GHz. The power spectrum of this source count distribution is estimated with the formalism in White & Majumdar (2004). The SZ background covariance is estimated from the simulations described in Shaw et al. (2007).

A different approach is taken for the bright point sources in the map. Any bright sources left in our map will cause ringing in the maps due to the matched filter used, which can give spurious high significance decrements in their vicinity. We take advantage of the fact that these sources show up as bright spots in our maps, while any SZ cluster will be a decrement at 150 GHz. We filter the 150 GHz map using a simple matched filter assuming isotropic noise and no signal filtering, and we flag every positive source above 5 sigma in the filtered map (totaling 47 sources in the ~ 40 square-degree BCS5h30 field). All pixels within a radius of 4 times the beam FWHM of the locations of these sources are set to a DC level defined to be the average of the pixels just outside the mask radius. To avoid any edge effects from the masking procedure, pixels within 8' of a masked source are flagged and excluded from later cluster finding. This technique proved adequate to avoid false detections near detected positive sources.

The instrumental and atmospheric noise properties of the maps are estimated using the two-dimensional power spectrum of jackknife noise maps (Sayers et al. 2008; Halverson et al. 2008). Under the assumption of stationarity in the map basis, the noise covariance matrix \tilde{N}_{noise} is diagonal in the Fourier domain and equal to the noise power spectrum. We construct as many independent jackknife maps as there are independent observations of the field by randomly multiplying each two hour observation of the field by ± 1 before coadding the full set of observations. We compute the 2d spatial power spectrum for each jackknife, and the quadrature mean of these power spectra is our estimate of \tilde{N}_{noise} .

2.3.3. Significance

The significance of a detection is estimated using the standard deviation of the filtered map pixels while excluding regions around bright point sources. As the integration time per pixel is a weak function of elevation, the scatter is estimated independently for each 1.5° band in elevation. The coverage of the selected region is uniform in azimuth. We define detection significance as the ratio of the peak of the candidate decrement divided by the RMS at the appropriate elevation.

2.4. False detection simulations

To assess the likelihood of false detections in our deep 150 GHz maps, we run the cluster detection pipeline over a series of simulated maps. The simulated maps include models of astrophysical contaminants (primary CMB and point sources) and noise. The CMB contribution to the simulated maps is a realization of the WMAP5

CMB power spectrum (Nolta et al. 2008). The point-source contribution is a spatially random distribution of sources drawn from models based on the Borys et al. (2003) counts for dusty protogalaxies and a version of the Toffolatti et al. (1998) counts for radio-loud AGN modified to match the DASI, CBI, and VSA counts at 30 GHz (Kovac et al. 2002; Mason et al. 2003; Cleary et al. 2005). Both the CMB and point-source contributions are spatially filtered to mimic the effect of our beams and most of our timestream processing. The effect of the common-mode subtraction is not included. The noise in the simulated maps is created using a jack-knife procedure identical to the one described in Section 2.3.2. As with the real data, clusters are searched for in each of fourteen filtered versions of each simulated map, using a β -model source template with $\beta = 1$ and θ_{core} ranging from 0.25' to 3.5' in 0.25' steps. In 100 simulated maps, we incur an average of 0.02 false detections per 40 square degrees for the signal-to-noise ratio of the least significant cluster candidate listed in Table 1 and Figure 1.

3. RESULTS

In this section, we present the four highest-significance cluster candidates found by our matched filter in the 150 GHz map of the ~ 40 square-degree BCS5h30 field. The highest-significance cluster in our field was previously found in the ROSAT-ESO Flux Limited X-ray (REFLEX) survey (Böhringer et al. 2004), in which it is identified as RXCJ0516.6-5430. The remaining three cluster candidates are new discoveries. Based on the simulated observations described in Section 2.4, there is roughly a 2% chance that our lowest-significance detection is false; the chances that any of the top 3 are false detections are significantly smaller than 1%.

To confirm that these detections have a thermal SZ spectrum, we look in filtered versions of our 95 GHz and 225 GHz maps at the locations of the 150 GHz detections. To check each object at the other two frequencies, we use a single-frequency, filtered map — created using a matched filter as described in Section 2.3 with the cluster spatial profile that produced the highest significance for that object in the 150 GHz map — and look at the single map pixel that corresponds to the center of the 150 GHz detection. The use of this method, and the fact that the pixel distributions in the filtered maps are Gaussian to a high degree of precision, allows us to easily interpret the signal-to-noise ratio (SNR) at the cluster candidate locations in the 95 GHz and 225 GHz maps.

The candidate locations, the SNR at that location in the filtered map in each of our observing bands, and the value of θ_{core} that maximized the SNR at 150 GHz, are presented in Table 1. We emphasize that this value of θ_{core} is the result of a one-parameter search over a very coarse grid using a model that may not be an accurate description of the detailed cluster morphology. It is also reported without a confidence interval. As such, it should be interpreted only as a rough measure of the angular scale of the cluster candidates. Images of all four candidates in the filtered maps are shown in Figure 1. Two things are immediately evident from the SNR values in the table and the images in the figure: 1) From the 150 GHz detections alone, all of the candidates are inconsistent with noise fluctuations, given the significance

of the detections. They are also inconsistent with emission from sources such as radio-loud AGN or dusty protogalaxies because of the polarity of the signal. 2) From the 95 and 225 GHz images and detection significances, all four detections appear consistent with thermal SZ signal and inconsistent with primary CMB, since each candidate is detected at reasonable significance in the 95 GHz map but not in the 225 GHz map.

We can make this second statement more quantitative. Using the relative depths of our 150 GHz and 95 GHz maps and the frequency dependence of the thermal SZ effect, we can make a rough prediction for the detection significance at 95 GHz from the 150 GHz detections. The RMS is approximately 4.8 times higher in CMB fluctuation temperature units in our 95 GHz map, but in those same units the thermal SZ signal should be approximately 1.6 times stronger at 95 GHz. Using these values, the predicted 95 GHz SNR values for our four candidates are -2.9, -2.4, -1.9, and -1.8, as compared to the observed values of -3.4, -3.9, -3.4, and -2.6 (cf., Table 1). By definition, the noise variance in the observed SNR values should be unity, by which it follows that the noise variance in the predicted 95 GHz SNR values should be $(1.6/4.8)^2$. Using these values of variance, a χ^2 test for the difference between the predicted and observed 95 GHz SNR values produces a probability to exceed (PTE) of 0.36. Because our 225 GHz band is very near the thermal SZ null, we should see effectively zero signal at cluster locations in our 225 GHz map. A χ^2 test for the observed SNR at 225 GHz produces a PTE of 0.24. We can do the same exercise for the hypothesis that the observed signal has a 2.7 K thermal spectrum (as would be the case for primary CMB fluctuations). In this case, the PTE for 95 GHz is still non-negligible (~ 0.007), because the difference between the spectra of SZ and primary CMB is not so great between 95 and 150 GHz. However, given the depth of the 225 GHz map (the RMS in CMB fluctuation temperature is approximately 2.5 times that in the 150 GHz map), we would expect SNR values of -3.4, -2.9, -2.3, and -2.2 at 225 GHz for a 2.7 K thermal spectrum. The PTE for this model given the observed SNR values at 225 GHz is less than 10^{-6} , giving strong evidence that the signal spectrum of our cluster candidates is inconsistent with primary CMB but consistent with thermal SZ.

3.1. X-ray counterparts

As previously mentioned, the highest-significance object in our sample (SPT-CL 0517-5430) was identified as a galaxy cluster in the REFLEX survey, which selected cluster candidates by correlating sources from a ROSAT All-Sky Survey (RASS, Truemper 1993) catalog with galaxy locations from optical data. Interestingly, we also find RASS counterparts to two of our other three cluster candidates, but these sources have not previously been considered as X-ray cluster candidates. The sources are found in the RASS Faint Source Catalog (RASS-FSC, Voges et al. 2000), and each lies within 1 arcminute of one of our SZ-detected clusters. 1RXS J054638.7-534434 lies 0.9 arcminutes northeast of SPT-CL 0547-5345, while 1RXS J050921.2-534159 lies 0.2 arcminutes northeast of SPT-CL 0509-5342 (see Figure 3). There are 105,924 sources in the RASS-FSC and 18,811 in the RASS Bright Source Catalog (RASS-BSC, Voges et al. 1999), which

TABLE 1
CLUSTER DETECTIONS

ID	R.A.	decl.	SNR at:			best θ_{core}
			150 GHz	95 GHz	225 GHz	
SPT-CL 0517-5430	79.144	-54.506	-8.8	-3.4	-0.4	1.5'
SPT-CL 0547-5345	86.650	-53.756	-7.4	-3.9	1.9	0.5'
SPT-CL 0509-5342	77.333	-53.702	-6.0	-3.4	0.1	1.25'
SPT-CL 0528-5300	82.011	-52.998	-5.5	-2.6	-1.3	0.5'

NOTE. — R.A. and decl. are in units of degrees (J2000).

NOTE. — The value of θ_{core} reported here is that which maximized the SNR of each cluster in the filtered 150 GHz maps (out of 14 values of θ_{core} in steps of 0.25') and should be interpreted only as a rough measure of that cluster's angular scale.

makes the likelihood of a chance superposition within 1 arcminute of a random location on the sky less than 0.3% (under the assumption that the RASS sources are evenly distributed on the sky). The RASS-FSC count rates in the broad energy band are 0.012 cts/s for 1RXS J054638.7-534434 and 0.035 cts/s for 1RXS J050921.2-534159. The count rates are both well below the flux threshold used in the REFLEX survey, which is approximately 0.08 cts/s in a slightly narrower energy band. Using the RASS-FSC exposure times and count rates, we estimate that both of these sources were detected with roughly 15 photons in the broad energy band. Neither of these sources would have been included in the Massive Cluster Survey (Ebeling et al. 2001), which only considered sources in the RASS-BSC. We find no X-ray counterpart in the literature or in publicly available catalogs for our cluster candidate SPT-CL 0528-5300.

3.1.1. Positional uncertainties in SPT SZ cluster detections

As discussed in Section 2.2.4, the absolute pointing of the SPT maps from which cluster candidates are extracted is accurate to roughly 10 arcseconds, as measured using sources in the PMN and SUMSS catalogs. However, the locations of the cluster candidates reported in Table 1 will not necessarily line up with the centers of the cluster optical or X-ray emission to that level of precision, because the different observations are sensitive to different combinations of physical properties of the cluster. Such a separation is particularly likely in extended systems and systems that have undergone recent mergers, such as SPT-CL 0517-5430 / RXCJ0516.6-5430 (Zhang et al. 2006). The position of the brightest cluster galaxy, the peak of the X-ray emission (which is proportional to electron column density squared), and the center of the SZ emission (which is linearly proportional to electron column density and is smoothed by the matched filter used for detection) can be offset by many times the positional uncertainty in any of the three measurements.

Figure 2 shows a minimally filtered version of the 150 GHz image in Figure 1, and it clearly shows the offset between center of the diffuse SZ emission and the deepest part of the SZ decrement. The X-ray emission should be strongly peaked in this deepest part of the decrement, and indeed this is where the reported REFLEX position is located.

3.2. Optical counterparts

We examine the galaxy distributions at the locations of the SZ selected clusters using deep, multiband opti-

cal images from the BCS. The BCS is a 60 night NOAO survey program (2005-2008) on the Blanco 4m that has uniformly imaged 75 deg² of the sky in SDSS *griz* bands in preparation for cluster finding with SPT and other millimeter-wave experiments. The depths in each band are tuned to follow cluster L_* galaxies to $z = 1$ with $>10\sigma$ detections. In addition to the large science fields, BCS covers 7 small fields that overlap large spectroscopic surveys so that the photometric redshifts (photo- z 's) using BCS data can be trained and tested using a sample of over 5,000 galaxies.

Figure 3 shows pseudo-color images created from deep BCS *gri* coadded images of the four systems. Early-type galaxies at similar redshift appear with similar color in these pseudo-color images. The clusters are arranged counter-clockwise by redshift starting in the upper left. In these images the galaxy populations in SPT-CL 0517-5430 and SPT-CL 0509-5342 are yellow, and the much fainter, higher-redshift populations in SPT-CL 0528-5300 and SPT-CL 0547-5345 are orange and red. In each image, the SPT position is marked with a 1-arcminute-diameter green circle.

We have used ANNz (Collister & Lahav 2004) photo- z 's and color-magnitude diagrams to probe for a cluster galaxy population and to provide rough redshift estimates for each of the SPT systems. A full analysis of the optical properties of these clusters that includes comparison to clusters selected by other means will appear in a separate paper. Here we provide a short summary of our findings.

In SPT-CL 0517-5430, the cluster that was previously detected in the REFLEX survey (Böhringer et al. 2004), there is a strong red sequence population apparent in $g-r$ versus r and a peak in the photo- z histogram. Both indicate a redshift of $z \sim 0.35$. The dominant elliptical is 0.5' to the northeast of the SPT position (see Figure 3).

In SPT-CL 0509-5342 the central dominant elliptical is clearly visible $\sim 0.25'$ to the southeast of the SPT position. This galaxy is marked by two and perhaps three strong gravitational lensing arcs. A large population of similarly colored and less luminous galaxies is apparent in the image and show up clearly as a red sequence in the $r-i$ versus i color-magnitude diagram. The red sequence indicates a cluster redshift of $z \sim 0.45$, while the photo- z histogram shows a peak around $z \sim 0.4$, but also several peaks at higher redshift.

SPT-CL 0528-5300 has a much fainter galaxy population at higher redshift, and it appears more concentrated on the sky. The cluster core is $\sim 0.4'$ east of the SPT

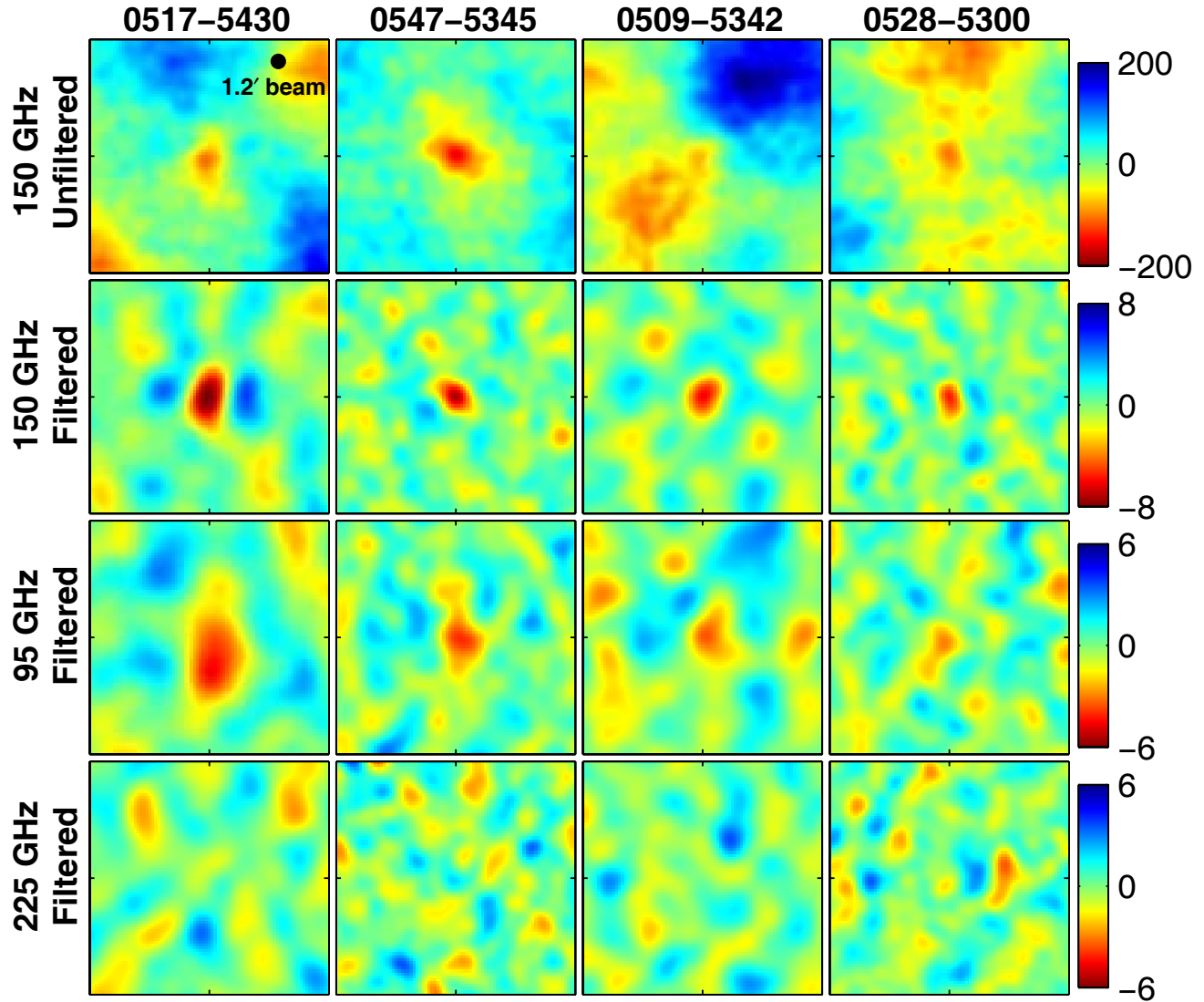


FIG. 1.— Images of four galaxy clusters found in the SPT SZ survey. In each panel, the region shown is a 20 by 20 arcminute box centered on the cluster. All images are oriented with north up and east to the left. In the top row, we show the unfiltered, beam-smoothed, 150 GHz map, and the scale has units of μK_{CMB} . The lower three rows show the 150, 95 and 225 GHz maps filtered using a $\beta = 1$ model with the θ_{core} listed in Table 1. The ringing on either side of the cluster in the 150 GHz filtered maps is an artifact of the filtering. The scale gives detection significance in σ . An SZ decrement will be stronger relative to primary CMB fluctuations at 95 GHz than it is at 150 GHz, but the increased noise in our 95 GHz maps results in a lower SNR at 95 GHz compared to 150. The detections at 95 GHz range in significance from 2.5σ to 3.9σ (see Table 1) and provide supporting evidence for the cluster detections. The null of the SZ spectrum is near 225 GHz, so there should be very little signal at cluster locations in the 225 GHz maps. Our 225 GHz maps are consistent with this prediction (see Table 1 and Section 3), providing another cross check that the data are consistent with SZ sources. The first cluster shown here, SPT-CL 0517-5430, was previously identified in the REFLEX X-ray cluster survey, in which it is identified as RXCJ0516.6-5430.

position, and the cluster galaxies appear orange in Figure 3. This cluster has a red sequence visible in $r - i$ versus i and in $i - z$ versus z suggesting a redshift of $z \sim 0.8$, again consistent with the location of a strong peak in the photo- z histogram.

SPT-CL 0547-5345 is the highest-redshift system; its galaxy population is faint and red in Figure 3. The cluster core is located $\sim 0.25'$ to the southeast of the SPT position. Inspection of the images reveals a large population of faint galaxies that are not readily apparent in the figure. The red sequence is not clearly detected for this cluster. We note, however, that the galaxies for this cluster are close to the detection limit and therefore

statistical uncertainties in their photometry are likely to be an issue. The photo- z histogram shows a peak at $z \sim 0.9$, very close to the high redshift range measured for the entire field. A feature that appears to be a strong gravitational lensing arc lies near the SPT circle to the southwest of the SPT position.

The BCS optical data reveal galaxy concentrations located within $0.5'$ of the SPT position for each of the four clusters. We find the cluster red sequence is present in all but the highest-redshift system and gravitational lensing arcs are present in two of the SPT systems, including the highest-redshift cluster.

We also note that the trend in cluster angular size — as

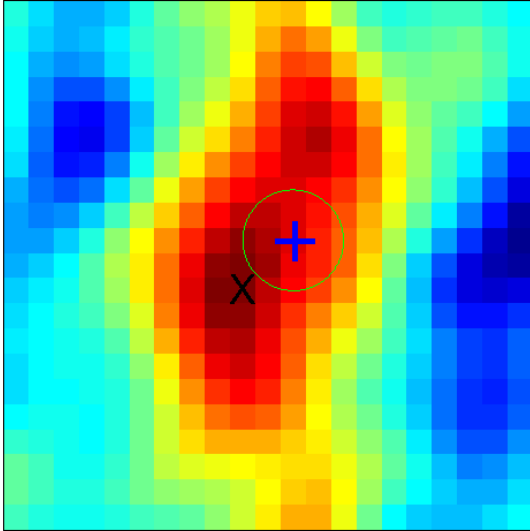


FIG. 2.— A minimally filtered (beam-smoothed to reduce pixel noise and high-passed to remove the primary CMB) 150 GHz image of SPT-CL 0517-5430, with colors and orientation as in the second row of Figure 1, but zoomed in such that the displayed region is 5 arcminutes on a side. The blue cross indicates the position of the peak of the output of the matched filter, i.e., the peak of the filtered 150 GHz image shown in Figure 1, which is also the position reported in Table 1. The black X indicates the position of RXCJ0516.6-5430, as reported in the REFLEX survey (Böhlinger et al. 2004). The green circle around the SZ detection center is 1 arcminute in diameter as in Figure 3, which also shows the REFLEX position.

evident from the images in Figure 1 and the rough estimate of θ_{core} in Table 1 — is consistent with the redshift estimates presented in this section. The two clusters estimated to lie at $z \gtrsim 0.8$ are noticeably more compact and prefer smaller values of θ_{core} than the clusters estimated to lie at $z \sim 0.4$.

4. CONCLUSIONS

In this paper, we have reported four high-significance detections of galaxy clusters made with the South Pole Telescope, three of which are new discoveries. These clusters were identified first as Sunyaev-Zel’dovich effect decrements in 150 GHz SPT maps. The presence of decrements at the corresponding positions in the 95 GHz maps, and lack of signal at the same positions in the 225 GHz maps, supports their identification as SZ sources. One of these four systems was previously identified as a cluster in the REFLEX X-ray cluster catalog. Two of the others have potential ROSAT All-Sky Survey Faint Source Catalog counterparts, but had not been identified as clusters. We have used data from the Blanco Cosmology Survey to produce pseudo-color optical images in the direction of the four SZ detections and find clear galaxy overdensities within 1 arcminute of the reported SPT positions. We also see evidence for strong gravitational lensing arcs in at least two of the optical images. Preliminary photometric redshift estimates indicate that two of the systems lie at moderate redshift

($z \sim 0.4$) and two at high redshift ($z \gtrsim 0.8$), consistent with the rough estimate of cluster angular scale from the SZ detections.

The cluster search presented in this paper was performed over a ~ 40 square-degree subfield of the SPT survey region observed in both the 2007 and 2008 seasons. The SPT is expanding the survey coverage, with an eventual target of ≥ 1000 square degrees. Future analysis will include additional data, as well as improvements to the data processing, calibration, and cluster identification algorithms. These initial cluster detections demonstrate the potential of SZ effect surveys, and in particular the SPT, to produce a sample of SZ-selected galaxy clusters. In combination with optical and X-ray data, these and future SZ-selected clusters will enable new explorations of galaxy cluster properties and constraints on cosmological models.

The SPT team gratefully acknowledges the contributions to the design and construction of the telescope by S. Busetti, E. Chauvin, T. Hughes, P. Huntley, and E. Nichols and his team of iron workers. We also thank the National Science Foundation (NSF) Office of Polar Programs, the United States Antarctic Program and the Raytheon Polar Services Company for their support of the project. We are grateful for professional support from the staff of the South Pole station. We acknowledge S. Alam, W. Barkhouse, M. Brodwin, L. Buckley-Geer, S. Hansen, W. High, H. Lin, Y-T Lin, A. Rest, J. Song, C. Smith and D. Tucker for their contribution to BCS data acquisition, and we acknowledge the DESDM team, which has developed the tools we used to process and calibrate the BCS data. We thank M. Brodwin, A. Gonzalez and C. Stubbs for their advice and contributions in the optical analysis. The BCS is supported by NSF awards AST 05-07688 and AST 07-08539. DESDM development is supported by NSF awards AST 07-15036 and AST 08-13534. We thank J. Leong, W. Lu, M. Runyan, D. Schwan, M. Sharp, and C. Greer for their early contributions to the SPT project and J. Joseph and C. Vu for their contributions to the electronics.

The South Pole Telescope is supported by the National Science Foundation through grants ANT-0638937 and ANT-0130612. Partial support is also provided by the NSF Physics Frontier Center grant PHY-0114422 to the Kavli Institute of Cosmological Physics at the University of Chicago, the Kavli Foundation and the Gordon and Betty Moore Foundation. The McGill group acknowledges funding from the National Sciences and Engineering Research Council of Canada, the Quebec Fonds de recherche sur la nature et les technologies, and the Canadian Institute for Advanced Research. The following individuals acknowledge additional support: A. Loehr from the Brinson Foundation, K. Schaffer from a KICP Fellowship, J. McMahon from a Fermi Fellowship, Z. Staniszewski from a GAAN Fellowship, and A.T. Lee from the Miller Institute for Basic Research in Science, University of California Berkeley.

REFERENCES

- Benson, B. A., Church, S. E., Ade, P. A. R., Bock, J. J., Ganga, K. M., Henson, C. N., & Thompson, K. L. 2004, *ApJ*, 617, 829
 Birkinshaw, M. 1999, *Physics Reports*, 310, 97
 Böhlinger, H., Schuecker, P., Guzzo, L., Collins, C. A., Voges, W., Cruddace, R. G., Ortiz-Gil, A., Chincarini, G., De Grandi, S., Edge, A. C., MacGillivray, H. T., Neumann, D. M., Schindler, S., & Shaver, P. 2004, *A&A*, 425, 367

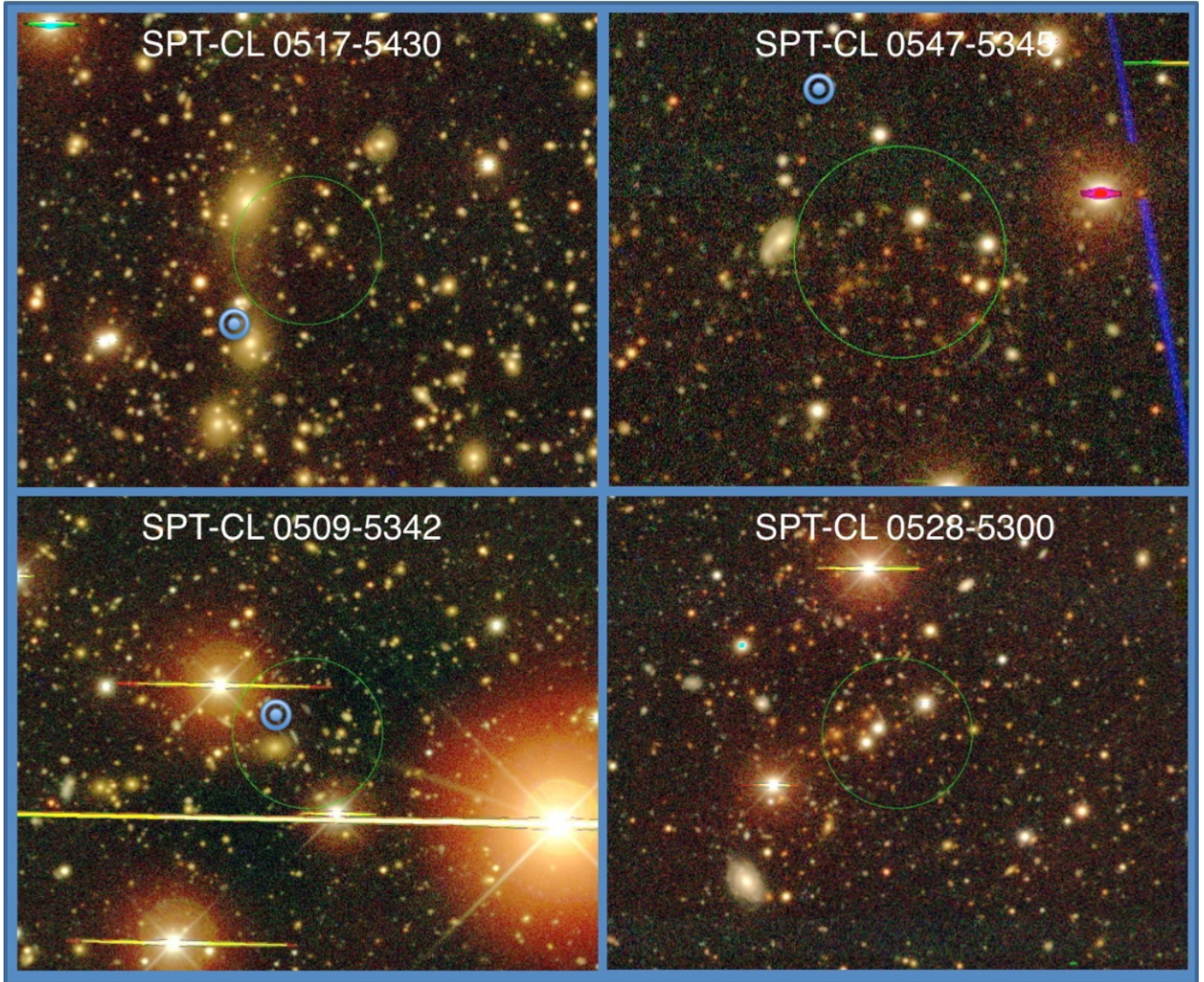


FIG. 3.— Pseudo-color optical images of the galaxy distributions toward the SPT clusters. All images are oriented with north up and east to the left, as in Figures 1 and 2. The SPT position is marked with a 1-arcminute-diameter green circle, as in Figure 2. Populations of early-type galaxies with similar color and central giant elliptical galaxies are found to lie within $0.5'$ of the SPT position of each system. Gravitational lensing arcs are apparent near the central galaxy in SPT-CL 0509-5342 and to the southwest of the cluster core in SPT-CL 0547-5345. The REFLEX position for SPT-CL 0517-5430 / RXCJ0516.6-5430 is indicated with a blue bullseye in the upper left panel, as are the positions of the possible RASS counterparts for SPT-CL 0547-5345 and SPT-CL 0509-5342 in their respective images.

Bonamente, M., Joy, M. K., LaRoque, S. J., Carlstrom, J. E., Reese, E. D., & Dawson, K. S. 2006, *ApJ*, 647, 25
 Borys, C., Chapman, S., Halpern, M., & Scott, D. 2003, *MNRAS*, 344, 385
 Calabretta, M. R. & Greisen, E. W. 2002, *A&A*, 395, 1077
 Carlstrom, J. E., Ade, P. A. R., Aird, K. A., Benson, B. A., Bleem, L. E., Busetti, S., Chang, C. L., Chauvin, E., Cho, H.-M., Crawford, T. M., Crites, A. T., Dobbs, M. A., Halverson, N. W., Heimsath, S., Hills, R. E., Holzzapfel, W. L., Joy, M., Keisler, R., Lanting, T. M., Lee, A. T., Leitch, E. M., Leong, J., Lu, W., Lueker, M., McMahon, J. J., Meyer, S. S., Mohr, J. J., Montroy, T. E., Padin, S., Plagge, T., Pryke, C., Ruhl, J. E., Schaffer, K. K., Schwan, D., Shirokoff, E., Spieler, H. G., Staniszewski, Z., Stark, A. A., & Vieira, J. D. 2008, in prep
 Carlstrom, J. E., Holder, G. P., & Reese, E. D. 2002, *ARA&A*, 40, 643

Cleary, K. A., Taylor, A. C., Waldram, E., Battye, R. A., Dickinson, C., Davies, R. D., Davis, R. J., Genova-Santos, R., Grainge, K., Jones, M. E., Kneissl, R., Pooley, G. G., Rebolo, R., Rubiño-Martín, J. A., Saunders, R. D. E., Scott, P. F., Slosar, A., Titterton, D., & Watson, R. A. 2005, *MNRAS*, 360, 340
 Coble, K., Ade, P. A. R., Bock, J. J., Bond, J. R., Borrill, J., Boscaleri, A., Contaldi, C. R., Crill, B. P., de Bernardis, P., Farese, P., Ganga, K., Giacometti, M., Hivon, E., Hristov, V. V., Iacoangeli, A., Jaffe, A. H., Jones, W. C., Lange, A. E., Martinis, L., Masi, S., Mason, P., Mausekopf, P. D., Melchiorri, A., Montroy, T., Netterfield, C. B., Nyman, L., Pascale, E., Piacentini, F., Pogosyan, D., Polenta, G., Pongetti, F., Prunet, S., Romeo, G., Ruhl, J. E., & Scaramuzzi, F. 2003, *ArXiv Astrophysics e-prints*, astro-ph/0301599
 Collister, A. A. & Lahav, O. 2004, *PASP*, 116, 345
 Ebeling, H., Edge, A. C., & Henry, J. P. 2001, *ApJ*, 553, 668
 Haehnelt, M. G. & Tegmark, M. 1996, *MNRAS*, 279, 545+
 Haiman, Z., Mohr, J. J., & Holder, G. P. 2001, *ApJ*, 553, 545

- Halverson, N. W., Lanting, T., Ade, P. A. R., Basu, K., Bender, A. N., Benson, B. A., Bertoldi, F., Cho, H., Chon, G., Clarke, J., Dobbs, M., Ferrusca, D., Guesten, R., Holzzapfel, W. L., Kovacs, A., Kennedy, J., Kermish, Z., Kneissl, R., Lee, A. T., Lueker, M., Mehl, J., Menten, K. M., Muders, D., Nord, M., Pacaud, F., Plagge, T., Reichardt, C., Richards, P. L., Schaaf, R., Schilke, P., Schuller, F., Schwan, D., Spieler, H., Tucker, C., Weiss, A., & Zahn, O. 2008, *ApJ*, submitted, arXiv:0807.4208
- Herranz, D., Sanz, J. L., Barreiro, R. B., & Martínez-González, E. 2002a, *ApJ*, 580, 610
- Herranz, D., Sanz, J. L., Hobson, M. P., Barreiro, R. B., Diego, J. M., Martínez-González, E., & Lasenby, A. N. 2002b, *MNRAS*, 336, 1057
- Holder, G., Haiman, Z., & Mohr, J. J. 2001, *ApJ*, 560, L111
- Holzzapfel, W. L., Carlstrom, J. E., Grego, L., Joy, M., & Reese, E. D. 2000, *ApJ*, 539, 67
- Jones, M. E., Edge, A. C., Grainge, K., Grainger, W. F., Kneissl, R., Pooley, G. G., Saunders, R., Miyoshi, S. J., Tsuruta, T., Yamashita, K., Tawara, Y., Furuzawa, A., Harada, A., & Hatsukade, I. 2005, *MNRAS*, 357, 518
- Kovac, J. M., Leitch, E. M., Pryke, C., Carlstrom, J. E., Halverson, N. W., & Holzzapfel, W. L. 2002, *Nature*, 420, 772
- Lima, M. & Hu, W. 2007, *Phys. Rev. D*, 76, 123013
- Majumdar, S. & Mohr, J. J. 2004, *ApJ*, 613, 41
- Mason, B. S., Pearson, T. J., Readhead, A. C. S., Shepherd, M. C., Sievers, J., Udomprasert, P. S., Cartwright, J. K., Farmer, A. J., Padin, S., Myers, S. T., Bond, J. R., Contaldi, C. R., Pen, U., Prunet, S., Pogosyan, D., Carlstrom, J. E., Kovac, J., Leitch, E. M., Pryke, C., Halverson, N. W., Holzzapfel, W. L., Altamirano, P., Bronfman, L., Casassus, S., May, J., & Joy, M. 2003, *ApJ*, 591, 540
- Mauch, T., Murphy, T., Buttery, H. J., Curran, J., Hunstead, R. W., Piestrzynski, B., Robertson, J. G., & Sadler, E. M. 2003, *MNRAS*, 342, 1117
- Melin, J.-B., Bartlett, J. G., & Delabrouille, J. 2005, *A&A*, 429, 417
- 2006, *A&A*, 459, 341
- Molnar, S. M., Haiman, Z., Birkinshaw, M., & Mushotzky, R. F. 2004, *ApJ*, 601, 22
- Motl, P. M., Hallman, E. J., Burns, J. O., & Norman, M. L. 2005, *ApJ*, 623, L63
- Nagai, D. 2006, *ApJ*, 650, 538
- Nagai, D., Kravtsov, A. V., & Vikhlinin, A. 2007, *ApJ*, 668, 1
- Navarro, J. F., Frenk, C. S., & White, S. D. M. 1996, *ApJ*, 462, 563
- 1997, *ApJ*, 490, 493
- Nolta, M. R., Dunkley, J., Hill, R. S., Hinshaw, G., Komatsu, E., Larson, D., Page, L., Spergel, D. N., Bennett, C. L., Gold, B., Jarosik, N., Odegard, N., Weiland, J. L., Wollack, E., Halpern, M., Kogut, A., Limon, M., Meyer, S. S., Tucker, G. S., & Wright, E. L. 2008, *ApJS*, submitted, arXiv:0803.0593
- Padin, S., Staniszewski, Z., Keisler, R., Joy, M., Stark, A. A., Ade, P. A. R., Aird, K. A., Benson, B. A., Bleem, L. E., Carlstrom, J. E., Chang, C. L., Crawford, T. M., Crites, A. T., Dobbs, M. A., Halverson, N. W., Heimsath, S., Hills, R. E., Holzzapfel, W. L., Lawrie, C., Lee, A. T., Leitch, E. M., Leong, J., Lu, W., Lueker, M., McMahon, J. J., Meyer, S. S., Mohr, J. J., Montroy, T. E., Plagge, T., Pryke, C., Ruhl, J. E., Schaffer, K. K., Shirokoff, E., Spieler, H. G., & Vieira, J. D. 2008, *Appl. Opt.*, 47, 4418
- Reichardt, C. L., Ade, P. A. R., Bock, J. J., Bond, J. R., Brevik, J. A., Contaldi, C. R., Daub, M. D., Dempsey, J. T., Goldstein, J. H., Holzzapfel, W. L., Kuo, C. L., Lange, A. E., Lueker, M., Newcomb, M., Peterson, J. B., Ruhl, J., Runyan, M. C., & Staniszewski, Z. 2008, *ApJ*, submitted, arXiv:0801.1491
- Richards, E. A., Fomalont, E. B., Kellerman, K. I., Partridge, R. B., & Windhorst, R. A. 1997, *AJ*, 113, 1475
- Ruhl, J., Ade, P. A. R., Carlstrom, J. E., Cho, H.-M., Crawford, T., Dobbs, M., Greer, C. H., Halverson, N. W., Holzzapfel, W. L., Lanting, T. M., Lee, A. T., Leitch, E. M., Leong, J., Lu, W., Lueker, M., Mehl, J., Meyer, S. S., Mohr, J. J., Padin, S., Plagge, T., Pryke, C., Runyan, M. C., Schwan, D., Sharp, M. K., Spieler, H., Staniszewski, Z., & Stark, A. A. 2004, in *Proc. SPIE*, Vol. 5498, Millimeter and Submillimeter Detectors for Astronomy II, ed. J. Zmuidzinas, W. S. Holland, & S. Withington (Bellingham: SPIE Optical Engineering Press), 11–29
- Runyan, M. C., Ade, P. A. R., Bhatia, R. S., Bock, J. J., Daub, M. D., Goldstein, J. H., Haynes, C. V., Holzzapfel, W. L., Kuo, C. L., Lange, A. E., Leong, J., Lueker, M., Newcomb, M., Peterson, J. B., Reichardt, C., Ruhl, J., Sirbi, G., Torbet, E., Tucker, C., Turner, A. D., & Woolsey, D. 2003, *ApJS*, 149, 265
- Sayers, J., Golwala, S. R., Rossinot, P., Ade, P. A. R., Aguirre, J. E., Bock, J. J., Edgington, S. F., Glenn, J., Goldin, A., Haig, D., Lange, A. E., Laurent, G. T., Maukopf, P. D., & Nguyen, H. T. 2008, *ApJ*, in press, arXiv:0805.3151
- Shaw, L. D., Holder, G. P., & Bode, P. 2007, *ApJ*, in press, arXiv:0710.4555
- Sunyaev, R. A. & Zeldovich, Y. B. 1970, *Comments on Astrophysics and Space Physics*, 2, 66
- 1972, *Comments on Astrophysics and Space Physics*, 4, 173
- Toffolatti, L., Argüeso Gomez, F., de Zotti, G., Mazzei, P., Franceschini, A., Danese, L., & Burigana, C. 1998, *MNRAS*, 297, 117
- Truemper, J. 1993, *Science*, 260, 1769
- Voges, W., Aschenbach, B., Boller, T., Bräuninger, H., Briel, U., Burkert, W., Dennerl, K., Englhauser, J., Gruber, R., Haberl, F., Hartner, G., Hasinger, G., Kürster, M., Pfeffermann, E., Pietsch, W., Predehl, P., Rosso, C., Schmitt, J. H. M. M., Trümper, J., & Zimmermann, H. U. 1999, *A&A*, 349, 389
- Voges, W., Aschenbach, B., Boller, T., Brauninger, H., Briel, U., Burkert, W., Dennerl, K., Englhauser, J., Gruber, R., Haberl, F., Hartner, G., Hasinger, G., Pfeffermann, E., Pietsch, W., Predehl, P., Schmitt, J., Trümper, J., & Zimmermann, U. 2000, *VizieR Online Data Catalog*, 9029, 0
- Wang, L. & Steinhardt, P. J. 1998, *ApJ*, 508, 483
- Wang, S., Khoury, J., Haiman, Z., & May, M. 2004, *Phys. Rev. D*, 70, 123008
- White, M. & Majumdar, S. 2004, *ApJ*, 602, 565
- Wright, A. E., Griffith, M. R., Burke, B. F., & Ekers, R. D. 1994, *ApJS*, 91, 111
- Zhang, Y.-Y., Böhringer, H., Finoguenov, A., Ikebe, Y., Matsushita, K., Schuecker, P., Guzzo, L., & Collins, C. A. 2006, *A&A*, 456, 55